# The role of oxygen termination of nanocrystalline diamond on immobilisation of BMP-2 and subsequent bone formation

F.R. Kloss [1], R. Gassner [1], J. Preiner [2], A. Ebner [2], K. Larsson [3], O. Hächl [1], T. Tuli [1], M. Rasse [1], D. Moser [4], K. Laimer [1], E.A. Nickel [1], G. Laschober [5], R. Brunauer [5], G. Klima [6], P. Hinterdorfer [2], D. Steinmüller-Nethl [7], G. Lepperdinger [5]

[1] Department of Cranio-Maxillofacial and Oral Surgery, Medical University of Innsbruck, Maximilianstr. 10, 6020 Innsbruck, Austria

[2] Institute for Biophysics, Johannes Kepler University of Linz, Altenbergerstr. 69, 4040 Linz, Austria

[3] Department of Materials Chemistry, Angstrom Laboratory, Uppsala University, Lägerhyddsvägen 1, Box 538, S-75121 Uppsala, Sweden

[4] University Hospital of Cranio-Maxillofacial and Oral Surgery, Medical School, University of Vienna, Währinger Gürtel 18-20, 1090 Vienna, Austria

[5] Institute for Biomedical Aging Research, Austrian Academy of Sciences, Rennweg 10, 6020 Innsbruck, Austria

[6] Department of Histology and Embryology, Müllerstrasse 59, 6020 Innsbruck, Austria

[7] ρ-BeSt coating GmbH, Exlgasse 20a, 6020 Innsbruck, Austria

**Corresponding author:** Dr. Dr. Frank Kloss Department of Cranio-Maxillofacial and Oral Surgery Medical University Innsbruck Maximilianstr. 10 6020 Innsbruck Austria e-mail: frank.kloss@i-med.ac.at

**Abstract**

Medical implants are increasingly often inserted into bone of frail patients, who are advanced in years. Due to age, severe trauma or pathology-related bone changes, osseous healing at the implant site is frequently limited. We were able to demonstrate that coating of endosseous implants with nanocrystalline diamond (NCD) allows stable functionalization by means of physisorption with BMP-2. Strong physisorption was shown to be directly related to the unique properties of NCD, and BMP-2 in its active form interacted strongest when NCD was oxygen-terminated. The binding of the protein was monitored under physiological conditions by single molecule force spectroscopy, and the respective adsorption energies were further substantiated by force-field-calculations. Implant surfaces refined in such a manner yielded enhanced osseointegration *in vivo*, when inserted into sheep calvaria. Our results further suggest that this technical advancement can be readily applied in clinical therapies with regard to bone healing, since primary human mesenchymal stromal cells strongly activated the expression of osteogenic markers when being cultivated on NCD physisorbed with physiological amounts of BMP-2.

**Keywords:** nano-crystalline diamond (NCD), physisorption, bone morphogenetic protein-2 (BMP-2), bone regeneration, mesenchymal stem cells

## Introduction

Only recently, the exceptional properties of diamond have been recognized to be not only of advantage in tool industry or tribology, but more than that it may also lead to improving advances when applied in life science, sensor technology or electronics. The deposition of thin films of nanocrystalline diamond (NCD) onto materials leaves the overall texture of specimen greatly unchanged while allocating a variety of properties of natural diamond to the substrate surface. Yet due to the nanotopography of NCD, the resulting surface is enlarged and in combination with further refinement, such as the termination of the dangling bonds of the carbon atoms, proliferation and differentiation of cells can be influenced in a controlled manner [1, 2]. Because the NCD surface is open to additional complex chemical refinement, it became conceivable for us to design medical implants that allow stable binding of molecules, such as bone morphogenetic protein-2 (BMP-2) [3, 4]. BMP-2 is capable of ectopic bone formation and has been approved for clinical use [5, 6]. In physiological settings, BMP-2 exerts its effects in nanogram doses [7], yet due to release from its site of application the recommended amounts applied to date are around 25 mg depending on the respective therapeutic regimen [5, 6]. Taking this into account and in order to prolong the effect of freely-diffusible growth factors, slow releasing systems have been put to test [8-10]. This way of practice however still incurs the risk of adverse effects, which in particular may affect the vascular system [11] or the immune system [12]. In an attempt to overcome these limitations we could demonstrate only recently that BMP-2 binds to oxygen-terminated NCD (O-NCD) in a highly stable, non-covalent manner, a procedure also known as physisorption [3]. In the present investigation we further corroborated these findings by performing detailed analytical measurements using atomic force microscopy (AFM). Moreover, by carrying out in depth theoretical modeling, we attempted to apprehend the nature of the protein-NCD

interaction at the atomic level. The effect of BMP-2 physisorbed to H- or O-terminated NCD was further tested *in vivo* by inserting implants into sheep calvaria. In order to extend our results from the animal experiment to the human system, we finally studied the osteogenic differentiation potential of primary human mesenchymal stromal cells grown on BMP-2 treated O-NCD covered implant surfaces as a substrate. The results presented in this contribution greatly suggest that this novel technique may be safely adopted for routine clinical therapies in the near future.

**Material and Methods:**

*Theoretical calculation:*

The three-dimensional structure of the BMP-2 homo-dimer [13] together with diamond as used in the present study was inapplicable as an input for quantum mechanical methods such as Density Functional Theory. Therefore, methods of classical molecular mechanics based on parameterized force fields were applied to overcome the problems with the size restrictions of quantum mechanical methods. The applied NCD-films show mainly (111) and (100) surface planes examined with xray diffraction. Reactivity of the (111) and (100) planes are known to behave equivalent with regard to adsorption. Theoretical calculations have shown that the bulk-diamond (100) surface is ideal to use for the present type of investigation [14]. Working along these lines and taking into account empirical data for molecules in isolation structural determinants at the atomic level were approximated resulting in simulations of thousands of atoms over nanoseconds of time and reliable predictions of a variety of physical properties. The ab initio force field (COMPASS (Condensedphase Optimized Molecular Potentials for Atomistic Simulation Studies; Accelrys, Inc., San Diego, USA)) was applied for an accurate and simultaneous prediction of structural properties for a broad range of molecules in isolation and in condensed phases as well as under a wide range of conditions of temperature and pressure was applied. The atomic charges were force field assigned in calculations with ultra-fine quality, with threshold values for optimization parameters such as energy, force and atomic displacement of $8.4 \times 10^{-5}$ kJ/mol, 0.04 kJ/mol/nm and $1.0 \times 10^{-6}$ nm, respectively. The summation method was atom based. Because the surface of many medical implants is composed of pure titanium or TiO2. and secondly in order to outline any qualitative effect taking place upon binding, the interaction of a BMP-2 homo-dimer with titanium, anatase and rutile in its (001) plane was modeled first. O-NCD was expected to be

superior to H-NCD [3], in particular with regard to BMP-2 surface bond strength at higher temperatures as well as for various surface concentrations of OH, and because the BMP-2/surface bond strength at room temperature and/or interfacial geometry will follow the calculated trend of bond energy, the calculations were performed at zero Kelvin, thus omitting the temperature dependent part (entropy, ΔS) of the free energy, ΔG:

$$\Delta G = \Delta H_{binding} + \Delta H_{conformation} - T\,(\Delta S_{rot,\ trans} + \Delta S_{flex} + \Delta S_{solvatation}) \qquad \text{(Equation 1)}$$

leading to the following interaction energy as base for the theoretical calculation:

$$\Delta H = H_{surface\text{-}dimer} - (H_{surface} - H_{dimer}) \qquad \text{(Equation 2)}$$

where $H_{surface\text{-}dimer}$, $H_{surface}$ and $H_{dimer}$ are the energies for the total complex and the reactants prior to the attachments. The interaction energy, ΔH, was divided into different terms depending on the type of bonding between the diamond surface and the BMP-2 homo-dimer: van der Waals (including H-bonds) and electrostatic energies.

*Preparation of the heteroepitaxial (001) diamond layer:*

Deposition of epitaxially oriented diamond grains on a silicon (001) single crystal substrate was done in a microwave plasma chemical vapor deposition (CVD) setup at a substrate temperature of 780°C, a microwave power of 1300 W and a gas pressure of 45 mbar. Oriented nucleation was induced by the bias enhanced nucleation procedure applying a negative voltage of - 210 V to the silicon substrate for 5 minutes in a gas mixture of 9% methane in hydrogen. During 18 hours growth, the process gas contained 7.5% methane and 1.25% carbon dioxide in hydrogen. The diamond surface was terminated with oxygen by thermal post-processing at 400°C for 4 hours with 21% oxygen.

*Preparation of nanocrystalline diamond (NCD) surfaces:*

Deposition of randomly oriented NCD films (500 to 800 nm thick and grain sizes of 5 to 20 nm) on titanium dental implants (length: 6 mm, diameter: 4.8 mm, surface topography: sandblasted, large grit and acid-etched (SLA) Straumann AG, Basel, Switzerland) was carried out as described recently [1]. The precursor gas was 3% methane in hydrogen. Nucleation was induced by ultrasonic mechanical seeding procedure. Eventually, the dangling bonds at the highly hydrophobic native NCD-surface (H-NCD) with a contact angle of ~120° were terminated with oxygen by thermal post-processing at 400°C for 4 hours with 21% oxygen, rendering the NCD-surface hydrophilic (O-NCD) (contact angles < 10°).

*Physisorption of BMP-2:*

BMP-2 (human, E.coli expressed, R&D, Minneapolis, USA) was dissolved in deionised water following the manufacturer's recommendation. NCD-coated substrates (heteroepitaxial diamond (001)) were incubated with BMP-2 (1 µg/mL) for 90 minutes in a humidified chamber. Subsequently, treated substrates were carefully rinsed with de-ionised water or phosphate-buffered saline (PBS).

*AFM imaging:*

Topographical images were acquired with the aid of a Pico Plus AFM equipped with a MACmode controller (Agilent Technologies, Tempe, AZ). Measurements were performed in PBS, pH 7.4 using a magnetically coated Cantilever (Agilent Technologies, Tempe, AZ) with a nominal force constant of 0.1 N/m.

*AFM force spectroscopy:*

The effective binding force of BMP-2 under physiologic conditions with respect to HNCD and O-NCD surfaces was quantitatively assessed using single molecule force

spectroscopy. BMP-2 was tethered to amino-functionalized silicon nitride AFM tips with a force-constant of 0.03 N/m (Veeco, Dourdan, France) via aldehyde-polyethylenglycol-N-hydroxysuccinimide as described previously [15]. The AFM tip with PEG-linked BMP-2 was approached and subsequently retracted with a velocity of 300 nm/s, and the deflection traces were recorded and transformed into force versus distance curves. As physisorption of BMP-2 is assumed being a stochastic process, statistical analysis of 1000 force-versus-distance curves on each surface (4 different positions per surface) were carried out. From each force-versusdistance curve, the unbinding force and the variance of the measuring noise (fluctuation of the baseline) were taken (as the mean and the variance) to generate a Gaussian distribution representing a single force value broadened by the intrinsic measurement noise. The experimental probability-density function was calculated by summing up the Gaussian distributions and the result was normalized with respect to the overall number of recorded curves [16].

*Surgical procedure and post operational treatment:*

Six healthy, 4 year-old female sheep weighing 70 ± 5 kg were fasted overnight while having free access to water. 0.5 mg atropine was administered and anaesthesia was induced with ketamin (Ketavet® 7-8 mg/kg body weight). After fiberoptic intubation during spontaneous respiration, the sheep were ventilated with a volume controlled ventilator (Draeger EV-A, Lübeck, Germany) with 35% O2/air at 14-18 breaths/minute and a tidal volume of 800 mL. Anaesthesia was maintained with Isoflurane (Forane®, Abbot, Vienna, Austria) and Ringer's solution (6 mL/kg/hr) was administered continuously throughout the operation to replace fluid loss during the surgical procedure. A sagittal incision was performed on the forehead to access the frontal bone. Twelve implant beds with a depth of 8-9 mm were prepared. During trepanation, special care was taken that the depth of the wound exceeded the implant length by 2-3 mm. This allowed us to follow bone healing

within the set wound together with de novo bone formation, the latter taking place directly at the apical site of the implant surface. The implants (Straumann AG, Basel, Switzerland) with and without NCD (rho-BeSt coating GmbH, Innsbruck, Austria) were distributed randomly, resulting in the following experimental groups: SLA titanium (control), H-NCD, O-NCD, H-NCD/BMP and O-NCD/BMP. After 3 days, 1 week and 4 weeks, two animals of each experimental group were sacrificed. Taken together five implants per experimental group and four implants of the control group at each time point were evaluated in detail. Bone specimens together with the inserted implants were embedded into Technovit 9100 neu (Heraeus Kulzer, Hanau, Germany). After embedding, specimens were bisected and one half was subjected to immunohistochemical analysis, while the other half underwent cutting-grinding resulting in 3 samples per specimen. The latter preparations were subsequently stained with Toluidine Blue O and the bone-to-implant contact ratio (BICR) as previously defined as the length of bone surface border in direct contact with the implant [5] was assessed for 15 different samples per time point and experimental group. However, BICR was solely determined at that surface lining, which prior to healing faced the open cavity. Hence only regions of de novo bone formation at the implant surface were taken into consideration. Immuno-histochemistry was performed using anti-BMP-2 antibody (H-51, rabbit polyclonal IgG; Santa Cruz Biotechnology Inc., Santa Cruz, CA) and a HRP-labeled anti-rabbit IgG followed by ACE+ staining (DAKO, Glostrup, Denmark).

*Cell Culture:*

Human bone-derived primary mesenchymal stromal cells (MSC) exhibiting osteogenic differentiation potential were cultivated on O-NCD-coated titanium that had been treated with BMP-2 in a manner comparable to the medical implants. MSC were isolated from the

iliac crest of systemically healthy individuals, which had been harvested for reconstructive bone surgery of defects within other areas of the body as described previously [17]. Briefly, a small biopsy of *substantia spongiosa osseum,* which otherwise would have been discarded based on necessary bone for molding and re-contouring prior to insertion into the recipient site was taken to further investigation under an Institutional Review Board-approved protocol after having obtained patients' written consent. After surgery, the bone was transferred into modified eagles medium (MEM) supplemented with 20% fetal calf serum (FCS), 100 units/mL penicillin, 100 µg/mL streptomycin, for transportation from the operation theatre to the clean room at room temperature. The biopsies were fragmented and marrow cells were isolated from pieces (20-100 $mm^3$) by centrifugation (400 x *g*, 1 minute). After centrifugation, the remaining pieces were treated with collagenase (2.5 mg/mL in MEM) for 2 hours at 37°C, 20% O2 and 5% CO2. Thereafter, the specimen was again centrifuged (400 x *g*, 1 minute). Cells were resuspended and loaded on a Ficoll-Paque Plus® gradient and centrifuged at 2,500 x *g* for 30 minutes. Cells were harvested from the interphase (density <1.075 g/mL), washed and collected by centrifugation (1,500 x *g*, 15 minutes). Cells were cultured at a density of 0.2 – 0.5 x $10^6$ cells/$cm^2$ at 5% $CO_2$ and 37°C (Heraeus, HeraCell 240). After 24 hours, the nonadherent cell fraction was removed by washing twice with PBS. After the primary culture had reached approximately 30 – 50% confluence, cells were washed twice with PBS, and subsequently treated with 0.05% trypsin / 1 mM EDTA for 3 – 5 minutes at 37°C. Cells were harvested, washed once in MEM and further expanded at a density of 50 cells/cm².

*RNA preparation and quantitative Reverse Transcription-Polymerase Chain Reaction* (qRT-PCR)*:* RNA was isolated from cells after homogenisation in 4.2 M guanidinium thiocyanate, phenol extraction and ethanol precipitation [17]. For qRT-PCR, cDNA was

synthesized from total RNA using RevertAid H Minus-MMuLV-RT (Fermentas, St. Leon-Roth, Germany) and oligo(dT) primer (MWG, Germany). The assays were performed on a LightCycler instrument (Roche, Austria) with the LC-FastStart DNA Master SYBR Green I Kit (Roche, Austria). The 15 µL reactions contained 2 µM forward and reverse primer and 3 mM MgCl2. After the activation of the enzyme at 95°C for 8 minutes, 50 cycles at 95°C for 15 seconds, 57°C for 8 seconds and 72°C for 15 seconds were performed. mRNA expression levels were calculated relative to eukaryotic translation elongation factor 1 alpha 1 (EEF1A1). Primer sequences and transcript IDs of the corresponding genes were as follows: SPARC/osteonectin (ENST00000231061) 5'-TCCCTGTACACTGGCAGTTC-3' / 5'-TCCAGGTCACAGGTCTCG-3'; PMF1/osteocalcin (ENST00000368272) 5'-ACACTCCTCGCCCTATTG-3' / 5'-TCCTGCTTGGACACAAAG-3', SPP1/osteopontin (ENST00000237623 / ENST00000359072 / ENST00000360804) 5'-ATGGCCGAGGTGATAGTG-3' / 5'-CATTCAACTCCTCGCTTTC-3'; IBSP/bone sialo protein-2 (ENST00000226284) 5'-CCGAAGAAAATGGAGATGACAG-3' / 5'-CCATAGCCCAGTGTTGTAGCA-3'; EEF1A1/elongation factor 1-alpha (ENST0000309268 / ENST0000316292 / ENST0000331523) 5'-CAAGTGCTAACATGCCTTGGT-3' / 5'-GAACAGTACCAATACCACCAATTT-3'.

**Statistics**

Data were statistically analysed using paired Student´s *t* test. Analyses were performed with SPSS (vs 15, SPSS Inc., Chicago, IL). The tests were two-sided with type 1 error probability of 0.05. Data are presented as mean values ± SD.

## Results

*Theoretical Calculation:*

The sum of the van-der-Waals and electrostatic interactions for different titanium substrates exhibited endothermic values (>0 kJ/mol) for all these compounds in the following order of decreasing endothermicity: TiO2(anatase)>TiO2(rutile)>Ti. This indicates that a BMP-2 homo-dimer will not bind to titanium surfaces. Regarding unrefined NCD (H-NCD), and O-NCD, our model assumed that besides van-der-Waals forces and H-bonds, also electrostatic interactions between the surface and BMP-2 account for binding. Under physiological conditions a water adlayer is present at NCD surfaces, which greatly influences the surface polarity and thus its degree of hydrophilicity [18]. Given that the diamond surface is completely terminated with OH and covered by a water adlayer (Figure 1), we calculated that the BMP-2 homo-dimer adsorbs in a highly exothermic reaction of about -850 kJ/mol, whereby the electrostatic interactions are contributing approximately 75%. In the case of H-NCD, BMP-2 binds only at a rate of about -250 kJ/mol (electrostatic interaction: 80%). Notably in both situations, due to the presence of the thin water interlayer, the adsorption energy changed by about - 200 kJ/mol.

*AFM imaging and force spectroscopy:*

AFM imaging was applied to reveal experimental evidence about the conformational state of BMP-2 when physisorbed onto O-NCD. This was feasible, because the (001) facets of heteroepitaxially oriented diamond crystallites are rather smooth (Figure 2A) so that single BMP-2 molecules could be clearly resolved using the AFM-technique [19]. Due to the size and morphological appearance, approximately 90 percent of the bound entities were distinguished as dimers (Figure 2 B,C). We furthermore experienced that bound BMP-2 was not removed, when directly touched with the AFM tip, even not when single

molecules had been imaged for several times. The interaction of BMP-2 with NCD surfaces was directly probed in force-versus-distance curves using AFM tips functionalized with BMP-2. BMP-2 showed strong interaction with O- and H-terminated diamond, whereas virtually no binding was observed on glass (Figure 3 A). A statistical validation of 1000 force-versus-distance curves yielded experimental probability-density-functions (pdfs) for unbinding forces. The latter were characterized by the most probable unbinding forces (maxima of pdfs') and their corresponding standard deviations. The interaction forces of 49.3 ± 20 pN were larger for O-terminated diamond compared to 38.2 ± 30 pN for H-terminated diamond (Figure 3B). Furthermore, the number of force-versus-distance curves containing a binding event (expressed as binding probabilities when normalized to the total number of force-versus-distance curves) of BMP-2 on O-terminated diamond was higher than on H-terminated diamond. With glass, only little interaction was observed (Figure 3 C).

*Osseointegration of BMP-2-treated, NCD-coated implants:*

In light of these results, we evaluated NCD with and without physisorbed BMP-2 *in vivo*. After three days, all wounds showed a high degree of hematoma. Using a specific antibody, which discriminates between ovine and recombinant BMP-2 in immuno-histochemical analysis, we examined both exogenous and endogenous BMP-2. Within developing bone and in the periost, BMP-2-like reactivity was detectable in all experimental groups (Figure 4). However, only in the case of O-NCD/BMP-covered implants, BMP-2 was also found right adjacent to the implant surface after 3 days and 1 week, presumably due to physisorbed BMP-2 delivered to these sites. One week post operation, cell numbers increased in the vicinity of those implants, which exposed SLA titanium, O-NCD as well as O-NCD/BMP and H-NCD/BMP to the wound, yet not in the

case of H-NCD-coated implants. H-NCD/BMP implants performed comparable to SLA titanium or O-NCD (Figure 4). In the surrounding of those cells, which had migrated into the space between bone and implant, decent amounts of BMP-2 were detectable (Figure 4). In the case of ONCD/BMP, not only high levels of BMP-2 were detectable in the cleft region, more than that, a higher number of putative osteoblasts were found in tight contact with the implant (Figure 4). These characteristic cells together with extracellular matrix (ECM) in close vicinity to the implant distinctively resembled early bone formation. Although BMP-2 was detectable in all experimental groups, the level of BMP-2 juxtaposed to O-NCD/BMP-coated implants was remarkably high, greatly suggesting that also *in vivo* BMP-2 remained physisorbed to O-NCD over a prolonged period. 4 weeks post operation, new bone was formed at the apex of the implant in all groups. BMP-2 levels at implantation sites were comparable to those of the surrounding osseous tissue.

One week post operation and Toluidine Blue O staining, in all specimens no gross histological differences were evident at sites of newly forming bone. However 4 weeks post operation, clear anatomical differences at the apical surface of the implant became apparent. Parts of the surface of SLA titanium, H-NCD and H-NCD/BMP were covered with accumulating fibrous tissue, whereas in the case of O-NCD/BMP, the implant was overlaid with a thick layer of mineralized osseous tissue (Figure 5). To rate the efficacy of de novo bone formation at the implant surface, the bone-implant-contact-ratio (BICR) was assessed (see graph depicted in Figure 6 A). When comparing O-NCD to SLA titanium implants as a control, BICR was increased, and it was even higher in the case of O-NCD/BMP. For H-NCD implants both with and without BMP-2, BICR was decreased. However, we also recognized that more bone mass was formed adjacent to O-NCD/BMP covered implants (Figure 6 B).

*Osteogenic induction of human mesenchymal stromal cells:*

After 7 days in culture, osteogenic differentiation was evaluated by monitoring the expression of molecular markers, such as the pre-osteoblastic protein, SPARC (osteonectin), IBSP (bone sialoprotein-2), as well as PMF1 (osteocalcin) and SPP-1 (osteopontin). In a first set of experiments, SPP-1 was found to be induced strongest (Figure 7A). In a subsequent series of experiments, increasing concentrations of BMP-2 were physisorbed to O-NCD prior to MSC cultivation. SPP-1 expression was activated in a concentration-dependent manner in those MSC, which had been cultured on O-NCD/BMP, while in those MSC, which were grown on plastic in the same culture well next to the test substrate, SPP-1 expression remained largely unchanged (Figure 7 B). This is indicative for BMP-2 remaining tightly bound to ONCD and after physisorption, if at all, only a minor amount appears to be freely diffusible in its active form. Interestingly however, MSC cultured on plastic adjacent to the O-NCD-coated substrate, which had been physisorbed with 1.5 µg/mL BMP-2, showed an increase in SPP-1 expression. This effect might be due to excessive BMP-2, which became released from the surface after initial physisorption.

**Discussion:**

Endosseous implants are widely used because they effectively support the functional and aesthetic rehabilitation in orthopaedics and maxillo-facial surgery. Although most implant types have been applied in several areas with high efficacy, the surface properties of endosseous implants were continuously improved over the last years in order to optimize healing performance as well as endurance within the patient's body. In this context it is important to point out that the patients' mean age, when receiving endosseous implants constantly increased during the previous years and for that reason, poor implant site conditions, which in many cases are due to age-associated bone changes became a more prevalent problem for therapeutic strategies [20]. Growth factors such as members of the BMP family are being applied in the clinics, in particular to improve bone healing in problematic trauma cases [5, 6, 21] as well as in reconstructive surgery [22]. Due to the fact that these growth factors are still administered in a rather crude fashion, the recommended dosages are far higher from those considered to be present under normal physiological conditions. Thus as a consequence unwanted systemic effects are possible [12]. These emerging problems can only be overcome by refining the method of application, e.g. by immobilizing drugs in cases where implants are used. Potential immobilization techniques are covalent binding or adsorption [9, 23-26]. Both techniques however exhibit considerable obstacles in a clinical setting. Covalent binding without complex chemistry in various sequential steps of protection and deprotection, which favor growth factor binding and minimize protein-protein crosslinking is hard to achieve by those who prepare for or perform surgery [24]. Alternatively, proteins may be immobilized to the surface of implants by adsorption. To date, many implant types are made of titanium or related alloys. These materials however exhibit only low to no protein adsorptive properties [9, 24]. A simple solution to this problem could be structural refinement or

coating of the surface with a layer of biocompatible material, which also binds biomolecules tightly. In line with this, we have only recently demonstrated that BMP-2 tightly binds to O-terminated NCD and physisorbed BMP-2 remains bioactive [3]. As assumed in this contribution, it appears likely that binding of BMP-2 to NCD preferentially occurs in an energetically minimized state, which concomitantly would not alter the protein's conformation. Opposed to that, no favorable interactions could be observed in the case of titanium both when performing modeling or physical assessments of interaction forces. This is in accordance with a report that certain nano-biomaterials do exhibit surface properties that support protein binding and more than that, could also be applied to sustain particular biological functions of cells [27]. Proteins may unfold when adsorbed on nanostructures compared to microstructures [28]. Adsorption to nano-biomaterials is firstly determined by a greatly enlarged surface-to-volume-ratio, which secondly specifies surface energy [26]. In the case of NCD, surface energy is furthermore established by exposition of defined characteristics of its termination, which in due course effectuates the adsorptive properties of the material. This issue can be addressed by modeling and employing theoretical calculations. For O-NCD, we observed that van-der-Waals forces, H-bonds and electrostatic interactions contribute to the accumulating binding forces. As a consequence, BMP-2 exhibits stronger binding energies on O-NCD compared to H-NCD.

Binding of biomolecules most often takes place in an aqueous environment, thus the effect of an water adlayer was included into the present calculations. Moreover, functionalized NCD surfaces appear to strongly bind water molecules. BMP-2 binding towards H- and O-terminated surfaces was therefore calculated in conjunction of a stable water adlayer present at the surface [28], and taking this into account, for BMP-2 on OH-terminated diamond the binding energies of - 859 kJ/mol were estimated. Binding of

BMP-2 when adsorbed on OH-terminated diamond can therefore be regarded as strong as if BMP-2 would have been attached in a covalent fashion. These considerations could be confirmed by means of AFM. The unbinding forces together with the overall binding probabilities of physisorbed BMP-2 on O-NCD were significantly higher compared to H-NCD. A conclusive proof of whether BMP-2, when being physisorbed to NCD is still capable of inducing ectopic bone formation is only offered by performing *in vivo* animal experiments [29-31]. Still it is poorly understood whether ECM acts as a buffer and due to slow release of BMP-2 a chemotactic gradient is being established, or whether cells solely respond to BMP, which is bound to components of the ECM and therefore is being presented in a complexed fashion to the corresponding surface receptor molecules [30]. This in mind, NCD-coated titanium was physisorbed with BMP-2 prior to engraftment into freshly injured bone. Intentionally, the apical site of the implant was not brought in direct contact with bone. Thereafter the effect of differently refined NCD with or without bound BMP-2 with respect to induction of bone formation was assessed. Notably, since physisorption was carried out with 1 µg/mL BMP-2, only sub microgram amounts of the growth factor were eventually introduced into the wound. This is in sharp contrast to the extent applied in the current clinical approaches.

One week after insertion, BMP-2 appeared to be solely present at those implant surfaces which were coated with O-NCD, strongly suggesting that stable binding of BMP-2 only took place on O-NCD and further persisted under *in vivo* conditions. This finding is consistent with what has been proposed by means of the theoretical calculations and had been measured with aid of AFM *in vitro*. Furthermore, the number of preosteoblasts in conjunction with collagen fibres, which were found in the wound bed at the basal part of the implant was increased. After 4 weeks after implantation this circumstance also yielded statistically significant elevated rates of BICR.in the case of O-NCD treated with BMP-2

when compared to O-NCD coated implants alone. This observation however implies that the effect was not entirely due to the activity of BMP-2 since O-NCD on its own, still improved healing when comparing the results of all experimental groups. These findings are in concordance with recent data, assuming that the positive effect of hydrophilic surface properties of implanted material exert a positive effect on osseointegration [32, 33]. Sufficed to say that O-NCD physisorbed with BMP-2 yielded the best results concerning the bone formation at the apex of the implant, it should be pointed out in this context that regardless of whether BMP-2 had been physisorbed to implants prior to insertion, H-NCD showed statistically significant decreased levels with respect to O-NCD and O-NCD treated with BMP-2 by resulting in a low BICR as well as in elevated levels of fibrous tissue formation adjacent to the implant. Notably, this effect was not found reverted in the case of BMP-2 treated H-NCD. This observation together with the results obtained after theoretical calculations and AFM measurements, suggest that only trace amounts of BMP-2 may bind to H-NCD and are most likely detaching from the implant surface soon after insertion.

As a first step in an attempt to translate these findings into a clinical application, we employed human primary MSC, which had been derived from bone of healthy individuals. *In vitro* these cells firmly attach to the surface of cell culture plastic, and there grown as a monolayer, MSCs can be efficiently induced by bioactive factors, e.g. BMP-2 to commence differentiation into osteoblasts. These particular cellular derivatives of MSC express specific molecular markers and also deposit characteristic ECM components together with high levels of calcium. These cells would normally also sense increasing doses of soluble BMP-2, which in due course results in a seemingly increased expression of various bone matrix proteins [34]. When we cultivated MSCs on O-NCD together with

BMP-2, a variety of molecular markers was activated. More than that, increasing amounts of BMP-2 resulted in a steady rise of the SPP-1 expression reaching a plateau when BMP-2 greater than 1 µg/mL had been physisorbed onto O-NCD. In the latter case, MSCs cultivated next to the NCD substrate also showed upregulation of SSP-1, which could well be due to BMP-2 released into the culture medium. In conclusion, protein binding to chemically refined NCD surfaces could be accurately monitored by means of AFM. Using that technique, we were able to rapidly assess the relative binding strength at the single-molecule level. Applied in future work, this regimen therefore eases further advancements of NCD surface refinement, in particular when designing specifically desirable surface properties with regard to binding of distinct proteins. Working along these lines, it became clear that BMP-2 stably immobilizes to NCD surfaces by physisorption. It appears highly likely that bone implants, which are functionalized in such a manner, can be safely applied for clinical purposes without implying the risk of adverse systemic side effects, because BMP-2 administered in this manner solely exhibit short-distance effects and thus enhances bone healing right at the implant sites. Due to the fact that biologically active factors can be easily immobilized by such means, appropriately low doses of bioactive factors are sufficient to yield the desirable biological effect. Accordingly, the use of expensive drugs in daily clinical life, e.g. cytokines, growth factors as well as other high-molecular-weight substances becomes affordable and most important in this context also safe. We therefore anticipate that implant surfaces when custom-tailored by NCD-coatings, provide a potential basis for implant functionalization with bioactive molecules.

**Acknowledgement**

KL and DS greatly acknowledge the RTN-project DRIVE (MRTN-CT-2004-512224) supported by the European Commission. The theoretical results were generated using the program package Material Studio, developed by Accelrys Inc.,San Diego. FK, RG and DS thank Straumann AG, Basel, Switzerland for providing the titanium dental implants and surgical equipment. FR and DS thank Martin Schreck, Institute for Physics, University of Augsburg, Germany for providing the epilayers of the diamond. GL is supported by the Jubilee Fund of the Austrian National Bank (#12518) and the Austrian Science Fund, FWF (NRN 093)

**References**

1. Kloss F, Najam-Ul-Haq M, Rainer M, Gassner R, Lepperdinger G, Huck CW, et al. Nano-crystalline diamond - an excellent platform for life science applications. J Nanosci Nanotechnol 2007;7:4581-4587.

2. Specht CG, Williams OA, Jackman RB, Schoepfer R. Ordered growth of neurons on diamond. Biomaterials 2004;25:4073-4078.

3. Steinmuller-Nethl D, Kloss FR, Najam-Ul-Haq M, Rainer M, Larsson K, Linsmeier C, et al. Strong binding of bioactive BMP-2 to nanocrystalline diamond by physisorption. Biomaterials 2006;27:4547-4556.

4. Härtl A, Schmich E, Garrido JA, Hernando J, Catharino SC, Walter S, et al. Protein-modified nanocrystalline diamond thin films for biosensor applications. Nat Mater 2004;3:736-742.

5. Dimar JR, Glassman SD, Burkus KJ, Carreon LY. Clinical outcomes and fusion success at 2 years of single-level instrumented posterolateral fusions with recombinant human bone morphogenetic protein-2/compression resistant matrix versus iliac crest bone graft. Spine 2006;31:2534-2539.

6. Govender S, Csimma C, Genant HK, Valentin-Opran A, Amit Y, Arbel R, et al. Recombinant human bone morphogenetic protein-2 for treatment of open tibial fractures: a prospective, controlled, randomized study of four hundred and fifty patients. J Bone Joint Surg Am 2002;84-A:2123-2134.

7. Sampath TK, Coughlin JE, Whetstone RM, Banach D, Corbett C, Ridge RJ, et al. Bovine osteogenic protein is composed of dimers of OP-1 and BMP-2A, two members of the transforming growth factor-beta superfamily. J Biol Chem 1990;265:13198-13205.

8. Sachse A, Wagner A, Keller M, Wagner O, Wetzel WD, Layher F, et al. Osteointegration of hydroxyapatite-titanium implants coated with nonglycosylated recombinant human bone morphogenetic protein-2 (BMP-2) in aged sheep. Bone

2005;37:699-710.

9. Liu Y, Huse RO, de Groot K, Buser D, Hunziker EB. Delivery mode and efficacy of BMP-2 in association with implants. J Dent Res 2007;86:84-89.

10. Jeon O, Song SJ, Kang SW, Putnam AJ, Kim BS. Enhancement of ectopic bone formation by bone morphogenetic protein-2 released from a heparin-conjugated poly(L-lactic-co-glycolic acid) scaffold. Biomaterials 2007;28:2763-2771.

11. Hruska KA, Mathew S, Saab G. Bone morphogenetic proteins in vascular calcification. Circ Res 2005;97:105-114.

12. Perri B, Cooper M, Lauryssen C, Anand N. Adverse swelling associated with use of rh-BMP-2 in anterior cervical discectomy and fusion: a case study. Spine J 2007;7:235-239.

13. Scheufler C, Sebald W, Hulsmeyer M. Crystal structure of human bone morphogenetic protein-2 at 2.7 A resolution. J Mol Biol 1999;287:103-115.

14. Larsson K. Surface properties of diamond under atmospheric conditions: A quantum mechanical approach. New Diamond Front Carbon Technol 2005;15:229-245.

15. Ebner A, Wildling L, Kamruzzahan AS, Rankl C, Wruss J, Hahn CD, et al. A new, simple method for linking of antibodies to atomic force microscopy tips. Bioconjug Chem 2007;18:1176-1184.

16. Bonanni B, Kamruzzahan AS, Bizzarri AR, Rankl C, Gruber HJ, Hinterdorfer P, et al. Single molecule recognition between cytochrome C 551 and gold-immobilized azurin by force spectroscopy. Biophys J 2005;89:2783-2791.

17. Fehrer C, Brunauer R, Laschober G, Unterluggauer H, Reitinger S, Kloss F, et al. Reduced oxygen tension attenuates differentiation capacity of human mesenchymal stem cells and prolongs their lifespan. Aging Cell 2007;6:745-757.

18. Härtl A, Garrido JA, Nowy S, Zimmermann R, Werner C, Horinek D, et al. The ion sensitivity of surface conductive single crystalline diamond. J Am Chem Soc

2007;129:1287-1292.

19. Rezek B, Shin D, Nakamura T, Nebel CE. Geometric properties of covalently bonded DNA on single-crystalline diamond. J Am Chem Soc 2006 Mar;128:3884-3885.

20. Kloss FR, Gassner R. Bone and aging: effects on the maxillofacial skeleton. Exp Gerontol 2006;41:123-129.

21. Friedlaender GE, Perry CR, Cole JD, Cook SD, Cierny G, Muschler GF, et al. Osteogenic protein-1 (bone morphogenetic protein-7) in the treatment of tibial nonunions. J Bone Joint Surg Am 2001;83-A Suppl 1:S151-158.

22. Warnke PH, Springer IN, Wiltfang J, Acil Y, Eufinger H, Wehmoller M, et al. Growth and transplantation of a custom vascularised bone graft in a man. Lancet 2004;364:766-770.

23. Xiao SJ, Textor M, Spencer ND, Wieland M, Keller B, Sigrist H. Immobilization of the cell-adhesive peptide Arg-Gly-Asp-Cys (RGDC) on titanium surfaces by covalent chemical attachment. J Mater Sci Mater Med 1997;8:867-872.

24. Nanci A, Wuest JD, Peru L, Brunet P, Sharma V, Zalzal S, et al. Chemical modification of titanium surfaces for covalent attachment of biological molecules. J Biomed Mater Res 1998;40:324-335.

25. Puleo DA, Kissling RA, Sheu MS. A technique to immobilize bioactive proteins, including bone morphogenetic protein-4 (BMP-4), on titanium alloy. Biomaterials 2002;23:2079-2087.

26. Williams SK, Kleinert LB, Hagen KM, Clapper DL. Covalent modification of porous implants using extracellular matrix proteins to accelerate neovascularization. J Biomed Mater Res A 2006;78:59-65.

27. Yao C, Perla V, McKenzie JL, Slamovich EB, Webster TJ. Anodized Ti and Ti6A14V possessing nanometer surface features enhance osteoblast adhesion. J Biomed Nanotechnol 2005;1:68-77.

28. Webster TJ, Schadler LS, Siegel RW, Bizios R. Mechanisms of enhanced osteoblast adhesion on nanophase alumina involve vitronectin. Tissue Eng 2001;7:291-301.

29. Urist MR. Bone: formation by autoinduction. Science 1965;150:893-899.

30. Sakou T. Bone morphogenetic proteins: from basic studies to clinical approaches. Bone 1998;22:591-603.

31. Whang K, Tsai DC, Nam EK, Aitken M, Sprague SM, Patel PK, et al. Ectopic bone formation via rhBMP-2 delivery from porous bioabsorbable polymer scaffolds. J Biomed Mater Res 1998;42:491-499.

32. Zhao G, Schwartz Z, Wieland M, Rupp F, Geis-Gerstorfer J, Cochran DL, et al. High surface energy enhances cell response to titanium substrate microstructure. J Biomed Mater Res A 2005;74:49-58.

33. Schwarz F, Herten M, Sager M, Wieland M, Dard M, Becker J. Histological and immunohistochemical analysis of initial and early osseous integration at chemically modified and conventional SLA titanium implants: preliminary results of a pilot study in dogs. Clin Oral Implants Res 2007;18:481-488.

34. van den Dolder J, de Ruijter AJ, Spauwen PH, Jansen JA. Observations on the effect of BMP-2 on rat bone marrow cells cultured on titanium substrates of different roughness. Biomaterials 2003;24:1853-1860.

**Figure Caption:**

**Figure 1: Model of terminated diamond / BMP-2 homo-dimer interaction**

Physisorbed BMP-2 remained active and exhibited high stability of binding sites without deforming the geometry and structure of the protein due to the relaxed position in adherent, energetically minimized state. Since the attachment of homodimer BMP-2 molecules has experimentally been observed to involve dimers in a position of about 3 nm above the diamond surface, a corresponding model for the force field calculation was applied. A thin water adlayer as expected on solid surfaces was integrated into the calculations. The resulting geometries for BMP-2 homo dimer on water-containing interfaces based on H- and OH-terminated diamond surfaces, are demonstrated in this figure: top: BMP-2 homo dimer on H-term. + water adlayer, bottom: BMP-2 homo dimer on OH-term. + water adlayer.

**Figure 2: Atomic force microscopy of BMP-2 physisorbed onto heteroepitaxial diamond film**

**(A)** Topography of bare heteroepitaxial diamond film at a cross-section depicted by the green line is displayed by the graph below. The surface was monitored at higher resolution before **(A, B)** and after **(C)** BMP-2 physisorption (false-color code is valid for both B and C). **(D)** 3-dimensional representation featuring the dimeric structure of bound BMP-2. The graph in the lower part of the panel displays the z-plane of the cross-sectioned area depicted by the green line.

**Figure 3: Monitoring of binding forces by AFM force spectroscopy**

**(A)** Using a BMP-2-functionalized AFM tip (aldehyde PEG linker), force spectroscopy was performed by recording force-versus-distance curves on (I) O-terminated diamond, (II) H-terminated diamond, and (III) glass. The red line shows the course of approaching the

surface; the blue depicts the force upon retraction of the AFM tip. At a distance of ~15 nm, which corresponds to the length of the stretched BMP-2/PEG conjugate, the protein unbinds from the surface with a force specific for the particular surface. The parabolic shape of the force curve before unbinding reflects the viscoelastic properties of the PEG linker. **(B)** Unbinding force distributions obtained for O-diamond (solid line), H-diamond (dashed line), and on glass (dash-dotted line) were acquired in PBS at room temperature. Probability density functions (pdf) were calculated on the bases of 1000 force-versus-distance measurements at 4 different positions of every specimen. **(C)** Histogram of the overall binding probabilities. Error-bars indicate standard deviations obtained from measurements on different surface positions.

**Figure 4: BMP-2 immune histochemistry after NCD implantation into bone**
Representative examples of immune-histochemical preparations derived from 3 days and 1 week post operation specimen, which had been reacted with an antibody detecting both human and ovine BMP-2. Regions adjacent to the apical site of the implant as highlighted in the scheme depicted at the upper left part of the panel are shown for titanium, hydrogen-NCD (H-NCD), and oxygen-terminated NCD (O-NCD). The latter was furthermore treated with 1 µg/mL BMP-2 (/BMP) prior to insertion into sheep calvarias.

**Figure 5**: **Histology of bone healing after implantation of BMP-2 coated NCD**
According to the depicted scheme at the left side of the panel, representative examples of Toluidine Blue O stained bone sections are presented. Specimens from all experimental groups (3 days, 1 and 4 weeks post operation) were processed by the cutting-grinding method. Connective tissue (c) adjacent to the implant was observed at titanium, H-NCD and H-NCD/BMP. Bars indicate 200 µm.

**Figure 6: Determination of bone-implant-contact-ratio after healing**

Bone-implant-contact-ratio (BICR) was only determined at the apical surface of the implant opposing the area of regeneration as shown in the diagram at the lower left site of the panel **(A)** and for those specimens that were derived from experimental animals, 4 weeks after implant insertion **(B)**.

**Figure 7: Induction of osteogenic markers in MSC cultured on NCD**

**(A)** Transcriptional activation of osteogenic markers in mesenchymal stromal cells, which were cultivated for 7 days on O-NCD that had been functionalized with 1 µg/mL BMP-2; SPARC: osteonectin, PMF1: osteocalcin, SPP-1: osteopontin, IBSP: bone sialoprotein 2. **(B)** Induction of SPP-1 in mesenchymal stromal cells, which were cultivated either on substrates functionalized with increasing amounts of BMP-2 (filled columns) or adhering on the plastic in the culture well adjacent to the NCD-coated substrates (open columns). All values were expressed as means ± standard error of the mean. Differences were considered significant when p as determined by a paired, two-sided Student's t test was less than 0.05.

Figure 1

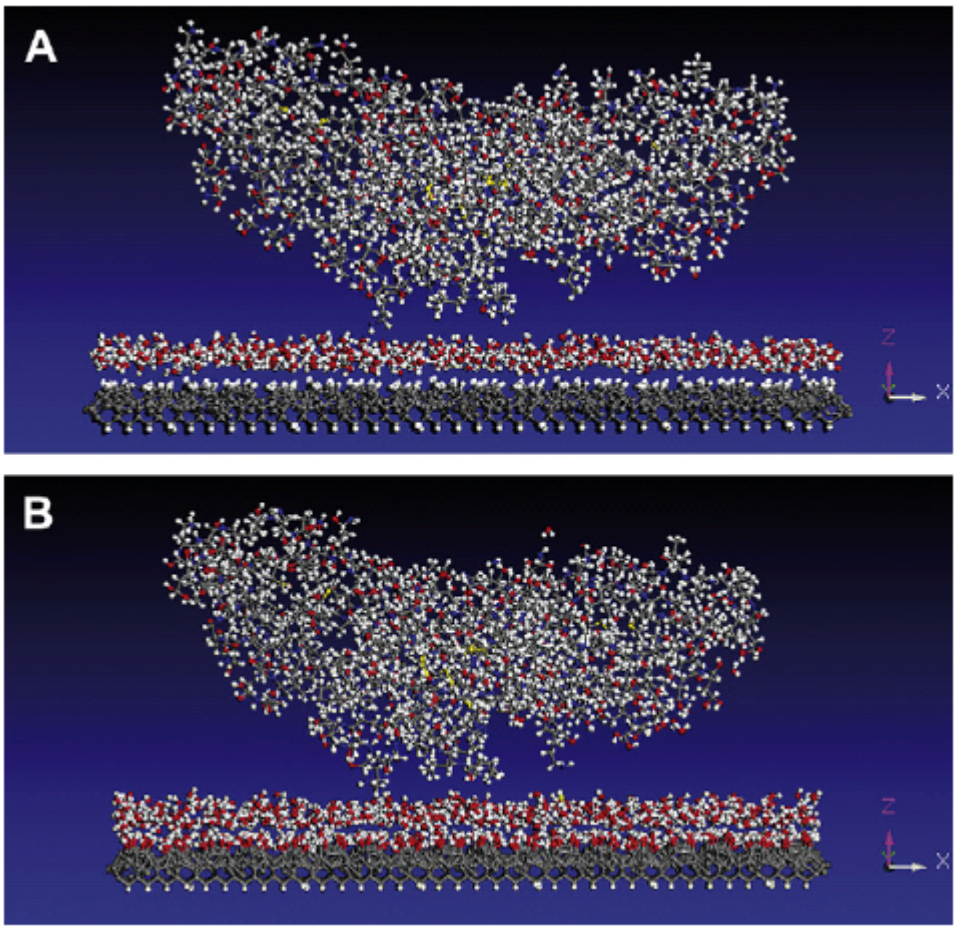


Figure 2

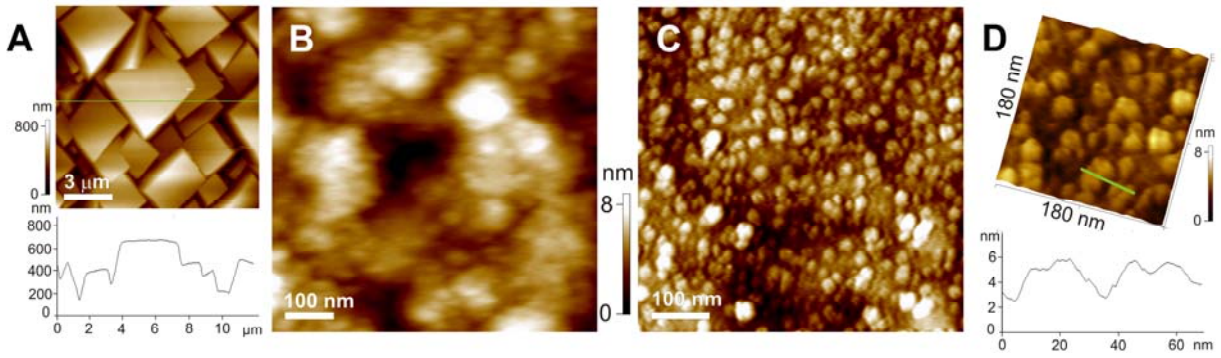

Figure 3

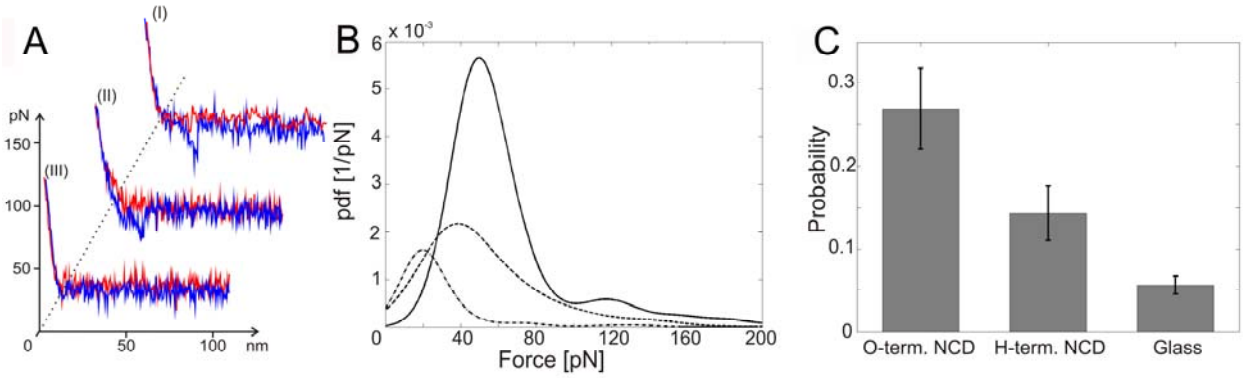
A
(I)
(II)
(III)
pN
150
100
50
0
50
100
nm
B
x 10-3
6
5
4
3
2
1
0
pdf [1/pN]
40
80
120
160
200
Force [pN]
C
0.3
0.2
0.1
0
Probability
O-term. NCD
H-term. NCD
Glass

Figure 4

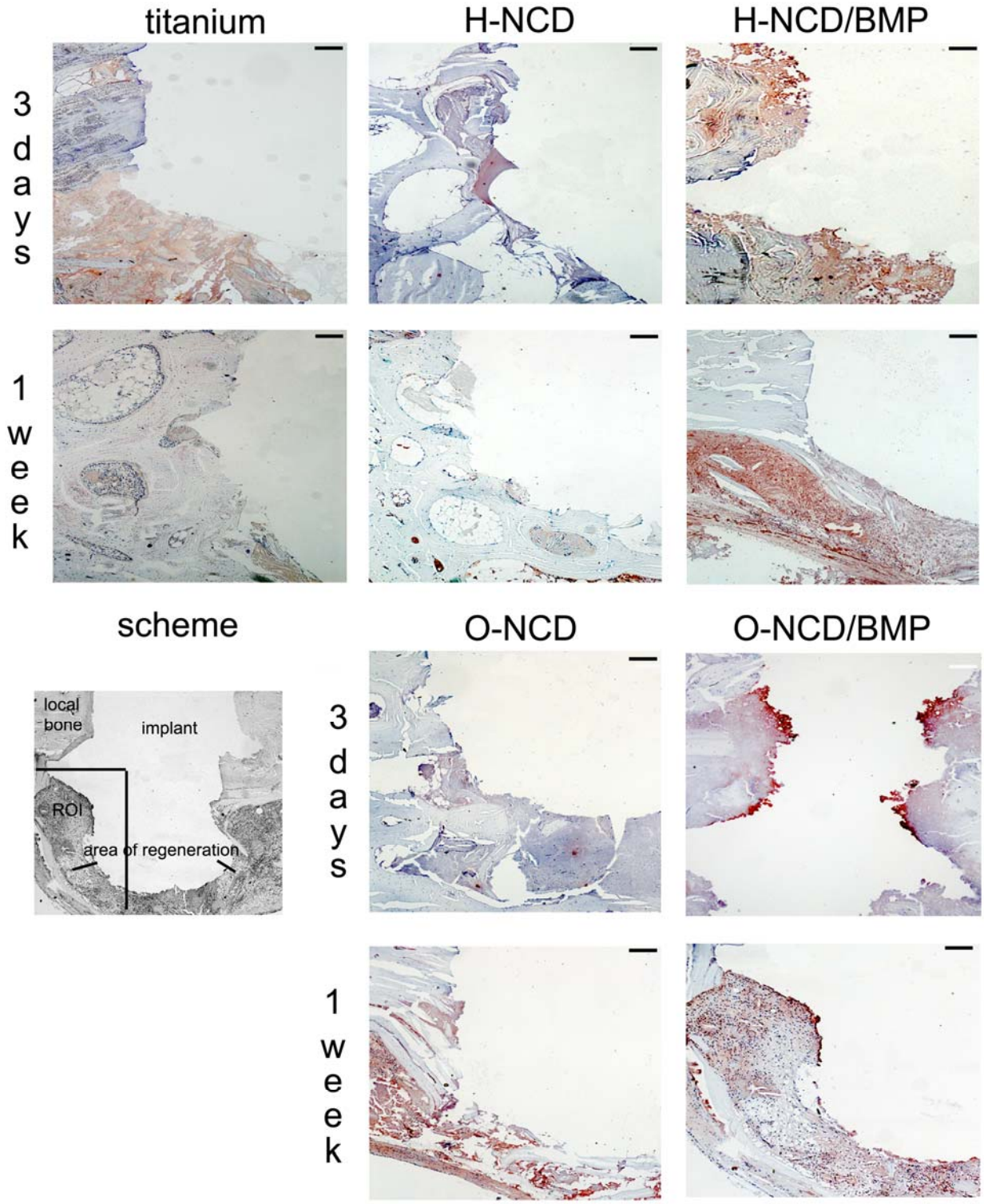
titanium
H-NCD
H-NCD/BMP
3 days
1 week
scheme
local bone
implant
ROI
area of regeneration
O-NCD
O-NCD/BMP
3 days
1 week

Figure 5

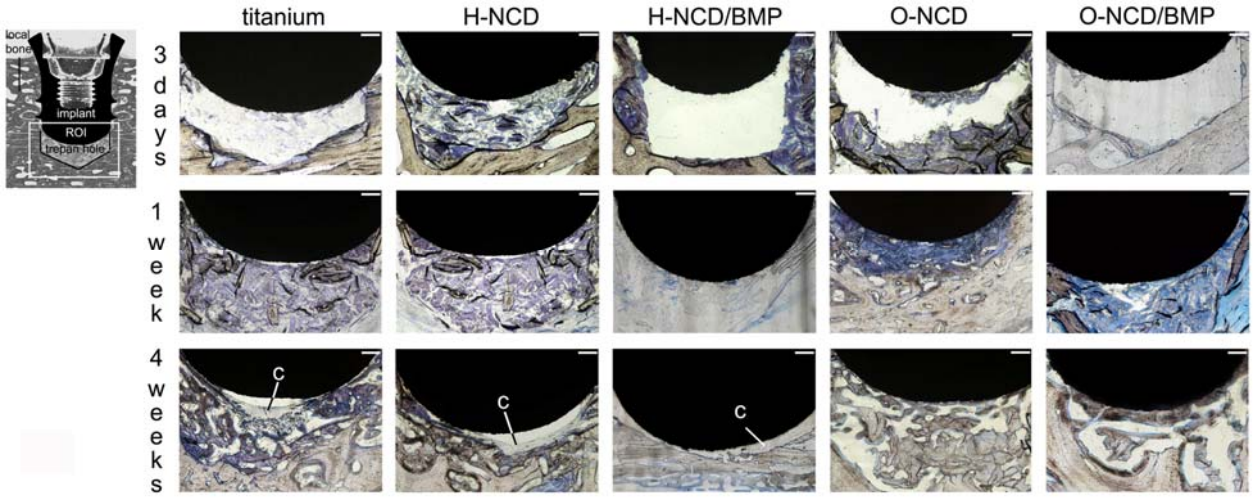


Figure 6

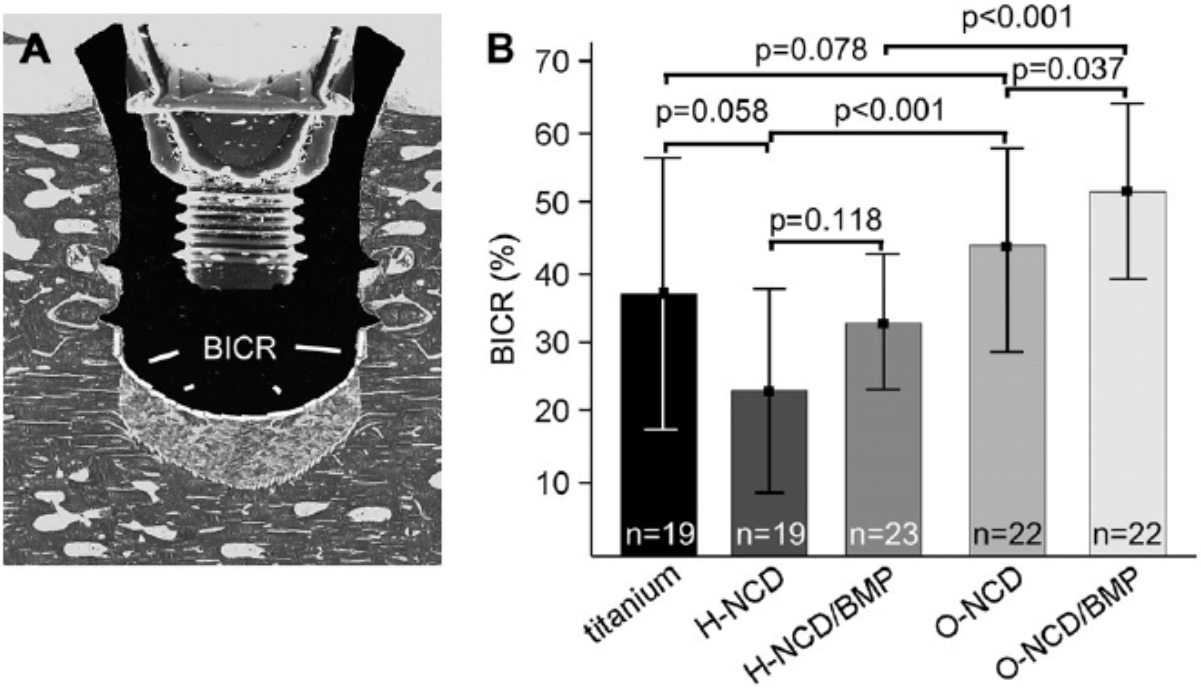

Figure 7

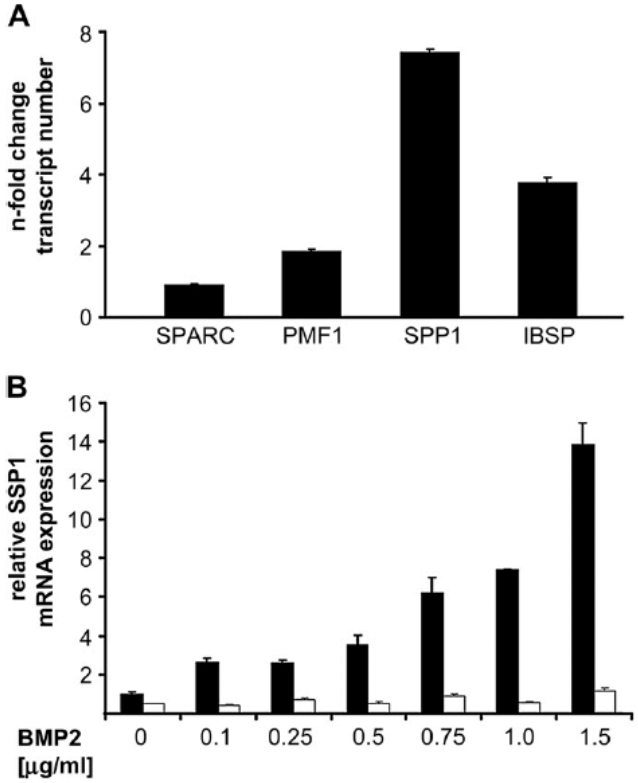
A
n-fold change transcript number
0
2
4
6
8
SPARC
PMF1
SPP1
IBSP
B
relative SSP1 mRNA expression
2
4
6
8
10
12
14
16
BMP2 [µg/ml]
0
0.1
0.25
0.5
0.75
1.0
1.5